Online PI Current Controller Tuning Based on Machine High-Frequency Parameters

Diego F. Laborda
University of Oviedo
Dept. of Elect., Computer & System Engineering
Gijón, Spain
dflaborda@uniovi.es

Juan Manuel Guerrero
University of Oviedo
Dept. of Elect., Computer & System Engineering
Gijón, Spain
guerrero@uniovi.es

Marcos Orviz Zapico
University of Oviedo
Dept. of Elect., Computer & System Engineering
Gijón, Spain
orvizmarcos@uniovi.es

Daniel Fernández
University of Oviedo
Dept. of Elect., Computer & System Engineering
Gijón, Spain
fernandezalodaniel@uniovi.es

David Díaz Reigosa
University of Oviedo
Dept. of Elect., Computer & System Engineering
Gijón, Spain
diazdavid@uniovi.es

Fernando Briz
University of Oviedo
Dept. of Elect., Computer & System Engineering
Gijón, Spain
fernando@isa.uniovi.es

***Abstract*— Synchronous PI current regulators are the preferred option for the current control of ac electric drives. The controller tuning requires knowledge of machine parameters that can change during normal operation, e.g. due to saturation and temperature variations, leading to changes in the current regulator dynamic response. This paper proposes the use of high-frequency signal injection (HFI) for parameter identification. This will enable online adaptation of the current regulator gains, eventually making their response robust against parameter variations.**

Keywords*— *PI Current Regulator, PI Current Controller, Tuning, High-Frequency Injection, HFI, Online Parameter Adaptation.

I. Introduction

Field-oriented control (FOC) normally uses Proportional Integral (PI) current controllers, as they guarantee zero steady-state error at the fundamental excitation frequency as well as a good dynamic response [1]. Controller tuning requires knowledge of the machine parameters [2], which are subjected to variations due to temperature and saturation. This can result in a degradation of the control performance. This can be avoided through robust control designs, e.g. sliding mode control [3], linear parameter varying [4], or internal mode control [5]. Alternatively, machine parameters can be estimated to adapt the controller gains. High-frequency injection (HFI) [6]–[12], extended Kalman filter (EKF) [13], model reference adaptive systems (MRAS) [14], neural networks (NNs) [15] or recursive least square (RLS) [16] have been reported in the literature. Table I summarizes their main characteristics.

HFI is a reliable method to estimate machine parameters [6]–[12]. The use of an HF signal for machine parameter estimation and PI controller tuning has been proposed in [10]; the method relies on spatial inductance mapping and does not allow online tuning (i.e. during normal operation of the machine) of the PI controllers.

This paper proposes an online tuning method for synchronous PI current controllers using a pulsating HF current signal superimposed to the fundamental excitation at 45º between *d*- and *q*-axes. Machine parameters will be estimated from its response to the HF signal. The proposed method can be used with any synchronous machine design, including interior permanent magnet synchronous machines (IPMSMs) and surface permanent magnet synchronous machines (SPMSMs), wound-rotor synchronous machines (WRSMs), and synchronous reluctance machines (SynRMs). This paper will focus on the IPMSMs case.

The paper is organized as follows: in Section II the fundamental model of PMSMs is shown; in Section III the PI current controller tuning method is explained; in Section IV the

TABLE I – ADVANTAGES AND DISADVANTAGES OF PARAMETER ESTIMATION METHODS

	Need of additional signals	Parameter sensitivity	No commissioning	Computational burden
HFI [6]–[12]	×	✓	✓	✓
EKF [13]	✓	✓	×	×
MRAS [14]	✓	×	✓	✓
NNs [15]	✓	✓	×	×
RLS [16]	✓	✓	×	×

This work was supported in part by the Research, Technological Development and Innovation Programs of the Spanish Ministry of Science and Innovation, under grant PID2019-106057RB-I00

HF inductance and resistance estimation are shown; in Sections V and VI simulation and experimental results are provided, respectively. Finally, conclusions are provided in Section VII.

II. Fundamental model of PMSMs

The fundamental model of a PMSM in a reference frame synchronous with the rotor is given by (1) [17], where p stands for the time derivative, R_d, R_q, L_d, and L_q are the d- and q-axis resistances and apparent (dc) d- and q-axis inductances respectively, ω_r is the rotor speed and λ_{pm} is the PM flux linkage. The d-axis is aligned with the PM flux.

$$\begin{bmatrix} v_{sd}^r \\ v_{sq}^r \end{bmatrix} = \begin{bmatrix} R_d & -\omega_r L_q \\ \omega_r L_d & R_q \end{bmatrix} \begin{bmatrix} i_{sd}^r \\ i_{sq}^r \end{bmatrix} + p \begin{bmatrix} L_d & 0 \\ 0 & L_q \end{bmatrix} \begin{bmatrix} i_{sd}^r \\ i_{sq}^r \end{bmatrix} + \begin{bmatrix} 0 \\ \lambda_{pm}\omega_r \end{bmatrix} \quad (1)$$

Inductances in (1) are commonly considered as constant values, therefore not being affected by the derivative operator [17]. However, in practice machine inductances vary due to saturation and temperature. Saturation can be modeled as shown in (2), which can be further reorganized as (3) by applying the chain rule for derivatives to (2). Finally, (4) is obtained, dynamic inductances being defined in (5). It is concluded that dynamic inductance should be used for current controller tuning if the magnetic saturation effect is to be considered. Temperature effects are not explicitly shown in the model, but its effects will be compensated by means of the parameter estimation method.

$$\begin{aligned} \begin{bmatrix} v_{sd}^r \\ v_{sq}^r \end{bmatrix} &= \begin{bmatrix} R_d & -\omega_r L_q \\ \omega_r L_d & R_q \end{bmatrix} \begin{bmatrix} i_{sd}^r \\ i_{sq}^r \end{bmatrix} + \\ &+ p\left(\begin{bmatrix} L_d & 0 \\ 0 & L_q \end{bmatrix} \right) \begin{bmatrix} i_{sd}^r \\ i_{sq}^r \end{bmatrix} + \begin{bmatrix} L_d & 0 \\ 0 & L_q \end{bmatrix} p\left(\begin{bmatrix} i_{sd}^r \\ i_{sq}^r \end{bmatrix} \right) + \begin{bmatrix} 0 \\ \lambda_{pm}\omega_r \end{bmatrix} \end{aligned} \quad (2)$$

$$\begin{aligned} \begin{bmatrix} v_{sd}^r \\ v_{sq}^r \end{bmatrix} &= \begin{bmatrix} R_d & -\omega_r L_q \\ \omega_r L_d & R_q \end{bmatrix} \begin{bmatrix} i_{sd}^r \\ i_{sq}^r \end{bmatrix} + \begin{bmatrix} \frac{\partial L_d}{\partial i_{sd}^r} & 0 \\ 0 & \frac{\partial L_q}{\partial i_{sq}^r} \end{bmatrix} p\left(\begin{bmatrix} i_{sd}^r \\ i_{sq}^r \end{bmatrix} \right) \cdot \begin{bmatrix} i_{sd}^r \\ i_{sq}^r \end{bmatrix} + \\ &+ \begin{bmatrix} L_d & 0 \\ 0 & L_q \end{bmatrix} p\left(\begin{bmatrix} i_{sd}^r \\ i_{sq}^r \end{bmatrix} \right) + \begin{bmatrix} 0 \\ \lambda_{pm}\omega_r \end{bmatrix} \end{aligned} \quad (3)$$

$$\begin{aligned} \begin{bmatrix} v_{sd}^r \\ v_{sq}^r \end{bmatrix} &= \begin{bmatrix} R_d & -\omega_r L_q \\ \omega_r L_d & R_q \end{bmatrix} \begin{bmatrix} i_{sd}^r \\ i_{sq}^r \end{bmatrix} + \begin{bmatrix} L_{dDyn} & 0 \\ 0 & L_{qDyn} \end{bmatrix} p \begin{bmatrix} i_{sd}^r \\ i_{sq}^r \end{bmatrix} + \\ &+ \begin{bmatrix} 0 \\ \lambda_{pm}\omega_r \end{bmatrix} \end{aligned} \quad (4)$$

$$\begin{bmatrix} L_{dDyn} & 0 \\ 0 & L_{qDyn} \end{bmatrix} = \begin{bmatrix} \frac{\partial L_d}{\partial i_{sd}^r} i_{sd}^r + L_d & 0 \\ 0 & \frac{\partial L_q}{\partial i_{sq}^r} i_{sq}^r + L_q \end{bmatrix} \quad (5)$$

III. PI current controller tuning

A. Synchronous PI current controller with cross-coupling decoupling

This section discusses PI current controller tuning using dynamic inductance and resistance. Zero-pole cancellation (ZPC) will be used. Fig. 1 schematically shows the current control scheme in the rotor synchronous reference frame. It is assumed that the back-EMF and cross-coupling terms of (1) are perfectly canceled [18].

The plant becomes (6) where the subscript x stands for d- or q-axis. (7) shows the PI current controller transfer function. PI controller parameters k_p and k_i are obtained from (8) and (9), where ω_{bw} is the desired bandwidth.

Fig. 2a shows the root locus of the control system shown in Fig. 1 in the case of an ideal ZPC. In the case of q-axis saturation due to q-axis current (positive or negative) injection, q-axis inductance will decrease; the resulting root locus being shown in Fig. 2b. An analogous effect will result from a stator resistance increase due to a stator temperature increase. In both cases, the resulting system settling time will be increased. In the case of negative d-axis current injection (i.e. flux weakening current), d-axis inductance will increase, the resulting root locus being shown in Fig. 2c. In this case, the resulting system settling time could be increased or create an undamped response, depending on the current controller gains.

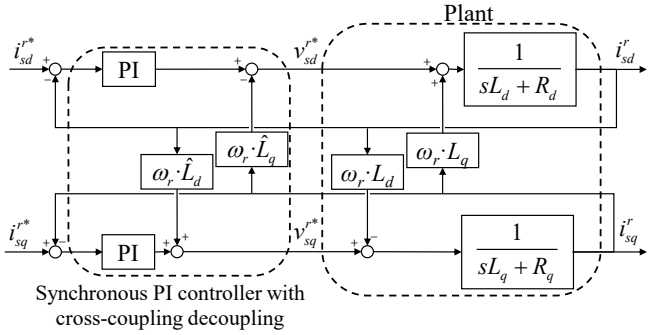

Fig. 1 - IPMSM control system scheme.

$$G(s) = \frac{1}{sL_x + R_x} \quad (6) \qquad C(s) = k_p + \frac{k_i}{s} \quad (7)$$

$$k_p = \omega_{bw}\hat{L}_x \quad (8) \qquad k_i = \omega_{bw}\hat{R}_x \quad (9)$$

Additionally, inductance variations affect the cross-coupling decoupling performance typically used with synchronous PI controllers, leading to larger settling time and undamped responses when the machine speed approaches to the current control bandwidth. To overcome this issue an improved synchronous PI controller structure for machines with magnetic reluctance ($L_d \neq L_q$), generalized from the complex-vector PI current regulators [18] is described in this paper along with the tuning procedure.

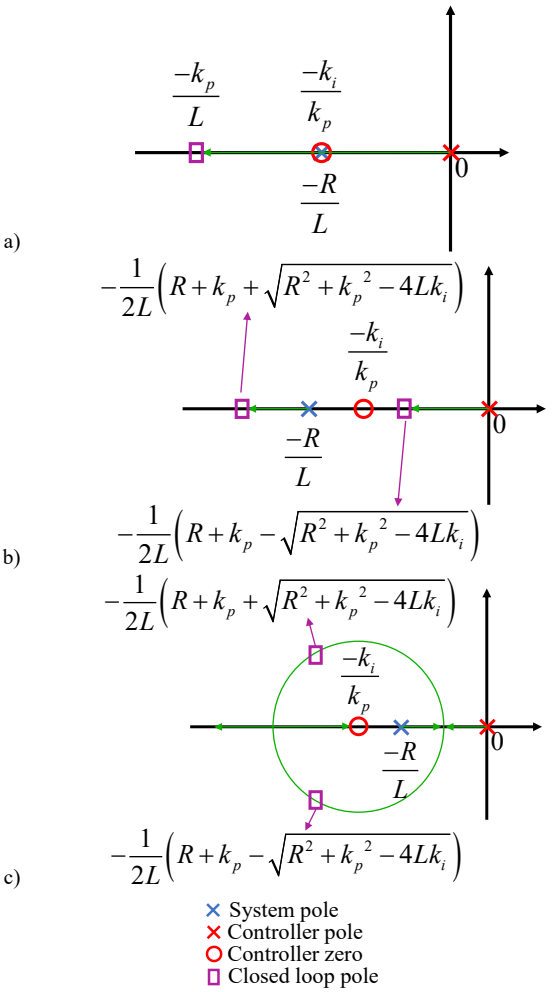

Fig. 2 - Root locus obtained by zero-pole cancellation. a) ideal, b) inductance decreased or resistance increased, and c) inductance increased.

B. *Matrix synchronous PI current controller*

A similar controller structure to that of (7) can be used with k_p and k_i being matrices defined in (10) and (11), where ω_{bw} is the desired bandwidth. This gain selection achieves ZPC in the cross-coupled system, similarly to the complex vector PI current controller for machines without reluctance ($L_d = L_q$) machines [18] and being analogous to the internal mode control (IMC) regulator presented in [19].

The block diagram of this controller is shown in Fig. 3. It is observed that the implementation is similar to the synchronous PI current controller with the addition of the cross-coupling branches.

$$k_i = k_p \begin{bmatrix} \frac{\hat{R}_d}{\hat{L}_d} & -\frac{\omega_r \hat{L}_q}{\hat{L}_d} \\ \frac{\omega_r \hat{L}_d}{\hat{L}_q} & \frac{\hat{R}_q}{\hat{L}_q} \end{bmatrix} \tag{10}$$

$$k_p = \begin{bmatrix} \omega_{bw}\hat{L}_d & 0 \\ 0 & \omega_{bw}\hat{L}_q \end{bmatrix} \tag{11}$$

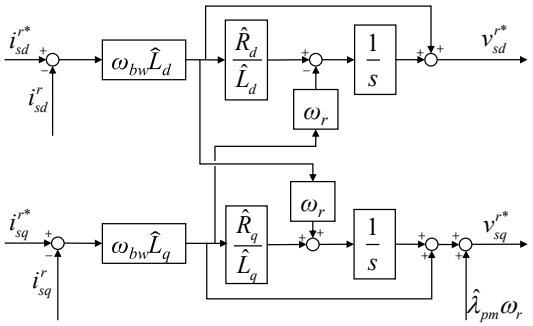

Fig. 3 – Matrix synchronous PI current controller structure.

Regardless of the structure or tuning technique used, accurate parameter (dynamic inductance and resistance) estimation is needed to guarantee both precise cross-coupling decoupling and the desired dynamic performance during machine normal operation.

IV. Dynamic Inductance and Resistance Estimation Using an HF Signal Injection

A. *Dynamic inductance and HF inductance*

The dynamic inductances are defined as the slope of the machine flux vs. current, around the operating point, and they can be obtained from (12) and (13). The injection of an HF current signal on top of the fundamental excitation creates small variations in machine flux, and voltages, around the operating point, HF inductances being possible to be calculated. If the HF current magnitude is small, the HF inductance values can be assumed to match with the dynamic inductances (5) [21], [22]. This is schematically shown in Fig. 4 for both *d*- and *q*-axes.

$$L_{dHF} \approx L_{dDyn} = \frac{\partial \lambda_{sd}^r}{\partial i_{sd}^r} = \frac{\partial (i_{sd}^r L_d + \lambda_{pm})}{\partial i_{sd}^r} = \frac{\partial L_d}{\partial i_{sd}^r} i_{sd}^r + L_d \tag{12}$$

$$L_{qHF} \approx L_{qDyn} = \frac{\partial \lambda_{sq}^r}{\partial i_{sq}^r} = \frac{\partial (i_{sq}^r L_q)}{\partial i_{sd}^r} = \frac{\partial L_q}{\partial i_{sq}^r} i_{sq}^r + L_q \tag{13}$$

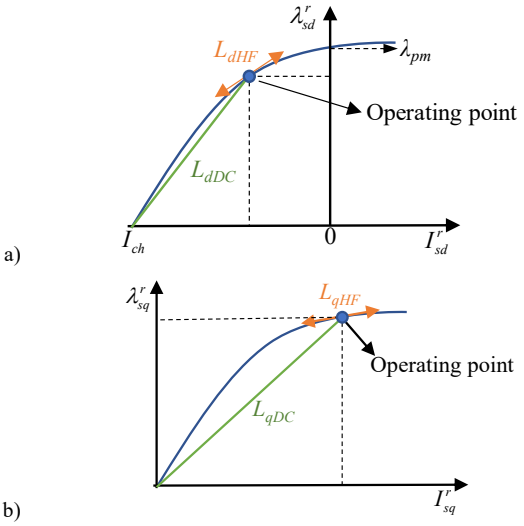

Fig. 4 - Schematic representation of dc (apparent) inductance and HF (dynamic) inductance for a) *d*-axis and b) *q*-axis.

B. HF inductance and resistance estimation

The HF model of a PMSM in a reference frame synchronous with the rotor is given by (14) [6], [20], where R_{dHF}, R_{qHF}, L_{dHF}, and L_{qHF} are the *d*- and *q*-axis HF resistances and inductances, respectively, i^r_{sdHF} and i^r_{sqHF} are the *d*- and *q*-axis HF currents and v^r_{sdHF} and v^r_{sqHF} are the *d*- and *q*-axis HF voltages.

$$\begin{bmatrix} v^r_{sdHF} \\ v^r_{sqHF} \end{bmatrix} = \begin{bmatrix} R_{dHF} & -\omega_r L_{qHF} \\ \omega_r L_{dHF} & R_{qHF} \end{bmatrix} \begin{bmatrix} i^r_{sdHF} \\ i^r_{sqHF} \end{bmatrix} + p \begin{bmatrix} L_{dHF} & 0 \\ 0 & L_{qHF} \end{bmatrix} \begin{bmatrix} i^r_{sdHF} \\ i^r_{sqHF} \end{bmatrix} \quad (14)$$

A pulsating HF current signal injected at 45º from the *d*-axis (15) can be used to estimate *d*- and *q*-axis HF stator resistances and inductances [6], where I^*_{HF} is the magnitude and ω_{HF} is the frequency of the injected signal. To inject the pulsating HF current signal on top of the fundamental excitation, a resonant controller in the synchronous reference frame is used as shown in Fig. 5. The *d*- and *q*-axis HF impedance are obtained from (16) and (17), respectively. The *d*- and *q*-axis HF inductances are obtained from (18) and (19), while the *d*- and *q*-axis HF resistances are obtained from (20) and (21) [6]. These equations are computed in the parameter estimation block shown in Fig. 5. The PI gains are then obtained using (8) and (9).

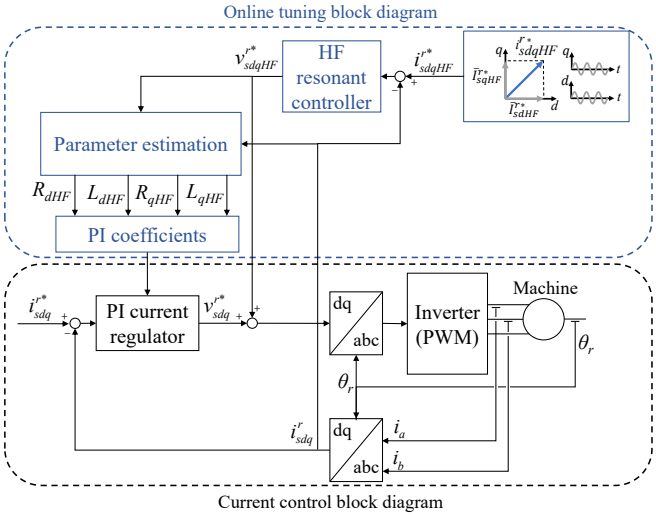

Fig. 5 - Proposed online PI current controller tuning based on HFI and current controller.

$$i^{r*}_{sdqHF} = \begin{bmatrix} \bar{I}^{r*}_{sdHF} \\ \bar{I}^{r*}_{sqHF} \end{bmatrix} = \begin{bmatrix} I^*_{HF}\cos(\omega_{HF}t) \\ I^*_{HF}\cos(\omega_{HF}t) \end{bmatrix} \quad (15)$$

$$Z_{dHF} = \frac{\bar{V}^{r*}_{sdHF}}{\bar{I}^{r}_{sdHF}} = R_{dHF} - \omega_r L_{qHF} + j\omega_{HF} L_{dHF} \quad (16)$$

$$Z_{qHF} = \frac{\bar{V}^{r*}_{sqHF}}{\bar{I}^{r}_{sqHF}} = R_{qHF} + \omega_r L_{dHF} + j\omega_{HF} L_{qHF} \quad (17)$$

$$L_{dHF} = \Im[Z_{dHF}]/\omega_{HF} \quad (18)$$

$$L_{qHF} = \Im[Z_{qHF}]/\omega_{HF} \quad (19)$$

$$R_{dHF} = \Re[Z_{dHF}] + \omega_r L_{qHF} \quad (20)$$

$$R_{qHF} = \Re[Z_{qHF}] - \omega_r L_{dHF} \quad (21)$$

V. Simulation Results

Finite element analysis (FEA) model of the IPMSM under test is shown in Fig. 6. The motor parameters are shown in Table II.

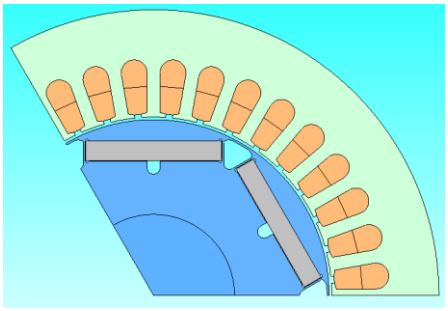

Fig. 6 - FEA model of tested IPMSM.

TABLE II- IPMSM Parameters

Rated Current	14 A
Rated Voltage	350 V
Rated Power	4 kW
Rated Speed	1000 r/min
Pole Pairs	3
Stator Resistance	1.2 Ω
d-axis inductance	4.2 mH
q-axis inductance	15 mH

In this section, the proposed method to adapt the controller gains is used for both synchronous PI current controller with cross-coupling decoupling (see Section III.A) and matrix synchronous PI current controller (see Section III.B). Their performance is tested by means of step reference tracking capabilities in both *d*- and *q*- axes. Their dynamic responses are compared with non-adaptive controllers and an ideal first-order response.

Non-adaptive current controllers are tuned with the nominal machine parameters (see Table II), while the adaptive current controllers obtain the machine parameters from HFI (see Section IV) at the operating point prior to the current step command. The HF current signal is injected at 45º between *d*- and *q*- axes with a magnitude of 0.05 p.u. and 1kHz of frequency. The selected bandwidth for tuning of all the tested controllers is 150 Hz. Relatively low bandwidths (150 Hz and 50 Hz) are used in this paper to emphasize the performance differences among current controller structures.

The operating point for the *d*- axis current step response test is I^r_{sd} = -1 p.u., I^r_{sq} = 0 p.u. , and the *d*- axis inductance is increased to 9.4 mH (+124%) by the FEA results. In a similar way, the operating point for the *q*- axis current step response test is I^r_{sd} = 0 p.u., I^r_{sq} = 0.9 p.u. , with a decrease of the *q*- axis inductance to 14 mH (-7%) by the FEA results. In both tests, the current step command value is +0.1 p.u.

Fig. 7 shows the *d*-axis current regulator response to a *d*-axis current step command. Fig. 7a shows the simulation results at zero speed condition providing an intrinsic decoupling between *d*- and *q*-axes, while Fig. 7b shows the simulation results at 300 r/min. Both non-adaptive controller responses are overlapped

and show larger settling time and overshot due to inductance variation, while both adaptive controllers maintain the desired settling time (also overlapping in the figure). There are no significant differences in the dynamic response between controller types or between different speed conditions exhibiting a correct decoupling between axes.

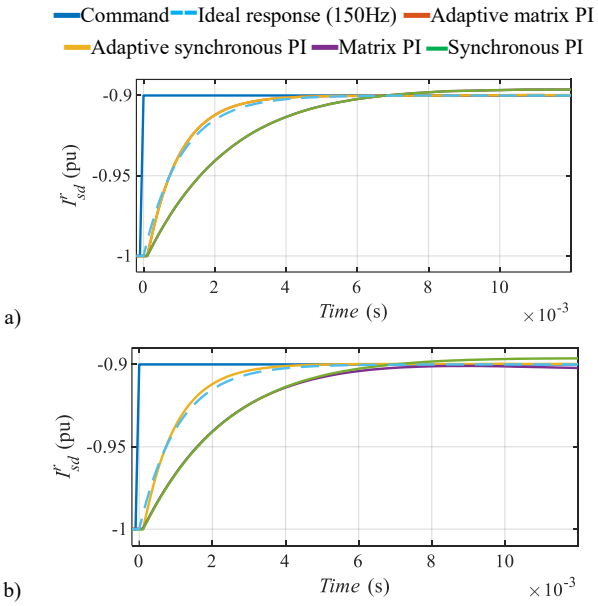

Fig. 7 - Simulation results. 0.1 p.u. *d*-axis step current response (L_d increased to 9.4mH ,+124%) a) at zero speed and b) at ω_r = 300r/min. ω_{bw}=2·π·150 rad/s. HFI: I_{HF} = 0.05 p.u., 1 kHz. Sampled at 10 kHz.

Fig. 8 shows an analogous experiment to Fig. 7 but for a *q*-axis current step command. In this case, the differences between the adaptive PI controllers and non-adaptive PI controllers are negligible (responses are overlapped in the figure) due to the smaller inductance variation in the *q*-axis at this operating point.

From these simulation results, it can be concluded that the adaptation of controller gains based on HF estimated parameters allow to maintain the desired bandwidth even when the machine inductance or resistance vary due to magnetic saturation or temperature variations.

The HF parameter estimation errors in simulations have shown to be around 3%, while the estimation error in experimental results is expected to be larger due to inverter non-linearities and noise. The quantification of estimation errors in experimental results is still ongoing research.

The estimation accuracy might affect the performance of adaptive controllers, therefore an estimation error of -20% in the *d*-axis inductance is artificially introduced in the next simulation results to test the impact of estimation errors in the performance of the method. Fig. 9 shows the *d*-axis current regulator response to a *d*-axis step command for adaptive matrix PI and adaptive synchronous PI current regulators when a -20% inductance estimation error is artificially introduced. The controller bandwidth has been lowered to 2π50 rad/s to amplify the effects of cross-coupling. It can be seen that inductance estimation errors have a larger effect when using the synchronous PI with cross-coupling decoupling (Section III.A) than matrix PI (Section III.B), as expected.

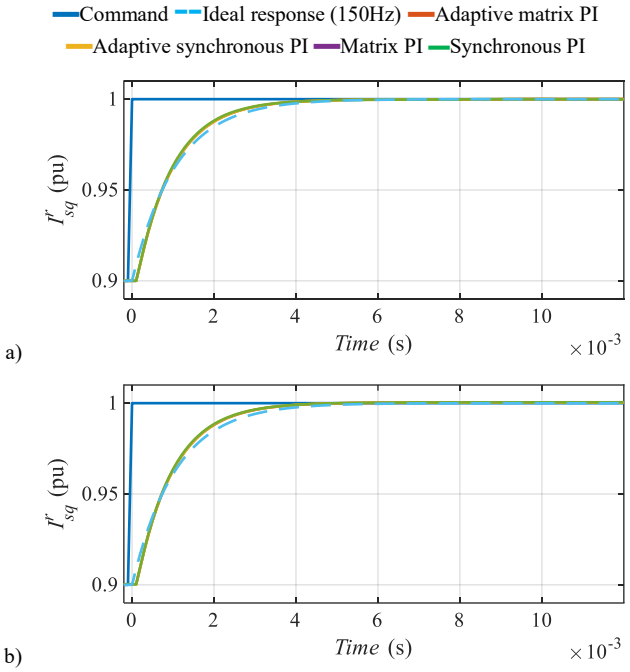

Fig. 8 - Simulation results. 0.1 p.u. *q*-axis step current response (L_q decreased to 14mH, -7%) a) at zero speed and b) at ω_r = 300r/min. ω_{bw}=2·π·150 rad/s. HFI: I_{HF} = 0.05 p.u., 1 kHz. Sampled at 10 kHz.

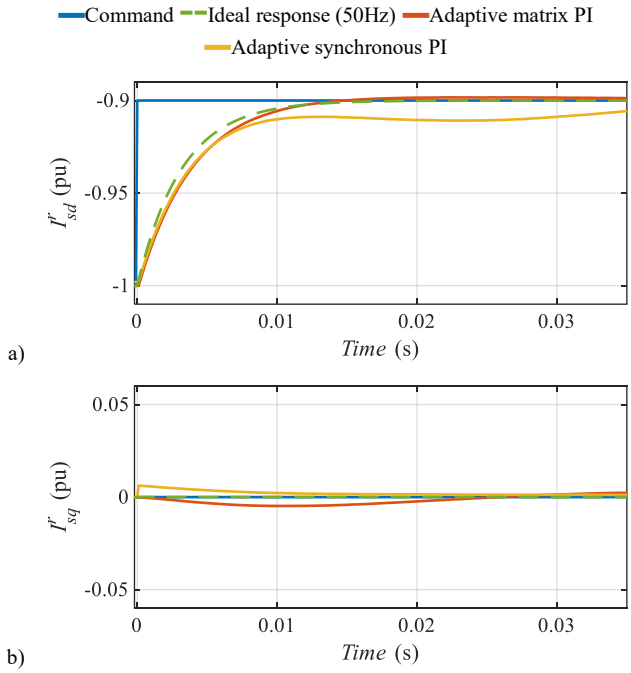

Fig. 9 - Simulation results. 0.1 p.u. *d*-axis step current response a) *d*-axis current response and b) *q*-axis current response with a -20% L_d estimation error, at ω_r = 300r/min. ω_{bw}=2·π·50 rad/s. HFI: I_{HF} = 0.05 p.u., 1 kHz. Sampled at 10 kHz.

VI. Preliminary Experimental Results

This section shows some preliminary experimental results of the proposed method. The IPMSM shown in Fig. 10 will be used

for the experimental verification of the method, its parameters can be seen in Table II.

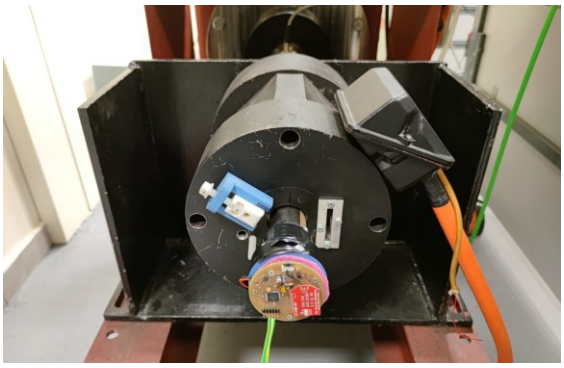

Fig. 10 – IPMSM used for experimental verification of the method.

Non-adaptive current controllers are tuned at the operating point: I^r_{sd} = -0.1 p.u., I^r_{sq} = 0 p.u. with a bandwidth of 150 Hz and their current step dynamic response is shown in Fig. 11. At this operating point, non-adaptive controllers have the desired dynamic response and both matrix and synchronous PI have overlapped responses.

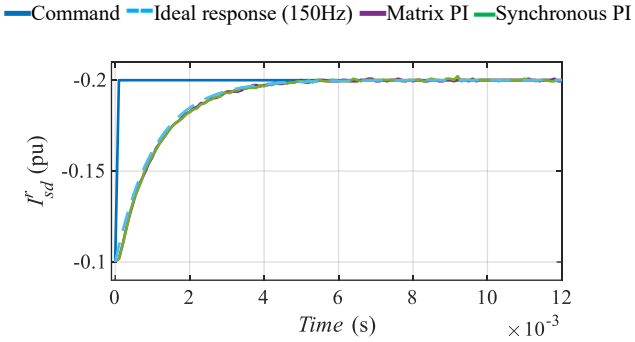

Fig. 11 – Experimental Results. -0.1 p.u. *d*-axis step current response, at zero speed. ω_{bw}=2·π·150 rad/s. Sampled at 10 kHz by the DSP.

The tuned non-adaptive controllers are used and compared with adaptive controllers at a different operating point (I^r_{sd} = -1 p.u., I^r_{sq} = 0 p.u.) where the magnetic saturation is lower (inductance is increased). First, an HF current signal of 0.05 p.u. and 1 kHz is injected between *d*- and *q*-axes to estimate both axis dynamic inductances and resistances at the operating point. After the machine parameters are estimated, a 0.1 p.u. step is applied to the *d*-axis current command. The results are compared in Fig. 12 with non-adaptive PI current controllers tuned at low current operating point (I^r_{sd} = -0.1 p.u., I^r_{sq}= 0 p.u.) and the first-order system ideal response. Both adaptive controllers meet the desired bandwidth and dynamic response, while non-adaptive controllers show a larger settling time and overshot, as expected. The non-adaptive controllers show faster dynamics compared with simulation results due to differences between FEA machine model and the actual machine parameters at the tested operating point. Nevertheless, the effect of the increased *d*-axis inductance is in good agreement with simulation results.

VII. Conclusions

A method for online tuning of PI current controllers based on HFI is proposed in this paper. It is demonstrated that dynamic inductances are responsible for machine dynamics. Simulation and preliminary experimental results have been presented to demonstrate the performance of the proposed method.

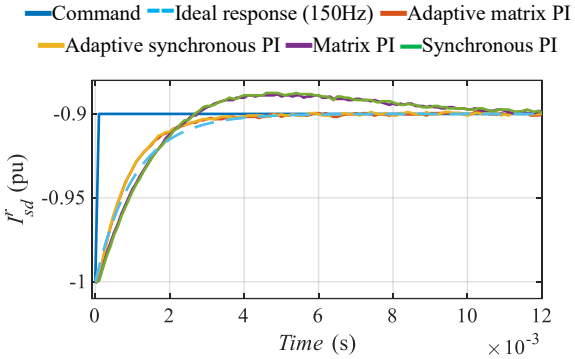

Fig. 12 – Experimental Results. 0.1 p.u. *d*-axis step current response, at zero speed. ω_{bw}=2·π·150 rad/s. HFI: I_{HF} = 0.05 p.u., 1 kHz. Sampled at 10 kHz by the DSP.

References

[1] T. M. Rowan and R. J. Kerkman, "A New Synchronous Current Regulator and an Analysis of Current-Regulated PWM Inverters," in *IEEE Trans. Ind. Appl.*, vol. IA-22, no. 4, pp. 678–690, Jul. 1986, doi: 10.1109/TIA.1986.4504778.

[2] A. G. Yepes, A. Vidal, J. Malvar, O. López, and J. Doval-Gandoy, "Tuning Method Aimed at Optimized Settling Time and Overshoot for Synchronous Proportional-Integral Current Control in Electric Machines," in *IEEE Trans. Power Electron.*, vol. 29, no. 6, pp. 3041–3054, Jun. 2014, doi: 10.1109/TPEL.2013.2276059.

[3] V. I. Utkin, "Sliding mode control design principles and applications to electric drives," in *IEEE Trans. Ind. Electron.*, vol. 40, no. 1, pp. 23–36, Feb. 1993, doi: 10.1109/41.184818.

[4] F. Amato, Robust Control of Linear Systems Subject to Uncertain Time-Varying Parameters. Berlin Heidelberg: Springer-Verlag, 2006.

[5] L. Harnefors and H.- Nee, "Robust current control of AC machines using the internal model control method," in *IAS '95. Conference Record of the 1995 IEEE Industry Applications Conference Thirtieth IAS Annual Meeting*, Oct. 1995, vol. 1, pp. 303–309 vol.1, doi: 10.1109/IAS.1995.530315.

[6] D. F. Laborda, D. D. Reigosa, D. Fernández, K. Sasaki, T. Kato, and F. Briz, "Enhanced Torque Estimation in Variable Leakage Flux PMSM Combining High and Low Frequency Signal Injection," in *2020 IEEE Energy Conversion Congress and Exposition (ECCE)*, Oct. 2020, pp. 1764–1771, doi: 10.1109/ECCE44975.2020.9235869.

[7] D. Raca, P. Garcia, D. Reigosa, F. Briz, and R. Lorenz, "A comparative analysis of pulsating vs. rotating vector carrier signal injection-based sensorless control," in *2008 Twenty-Third Annual IEEE Applied Power Electronics Conference and Exposition*, Feb. 2008, pp. 879–885, doi: 10.1109/APEC.2008.4522824.

[8] Y. G. Kang, D. Reigosa, B. Sarlioglu, and R. D. Lorenz, "*D*- and *Q*-Axis Inductance Estimation and Self-Sensing Condition Monitoring Using 45o Angle High-Frequency Injection," in *IEEE Trans. Ind. Appl.*, vol. 57, no. 1, pp. 506–515, Jan. 2021, doi: 10.1109/TIA.2020.3029993.

[9] M. Martinez, D. Reigosa, D. Fernández, J. M. Guerrero, and F. Briz, "Enhancement of Permanent-Magnet Synchronous Machines Torque Estimation Using Pulsating High-Frequency Current Injection," in *IEEE Trans. Ind. Appl.*, vol. 56, no. 1, pp. 358–366, Jan. 2020, doi: 10.1109/TIA.2019.2954297.

[10] F. Erturk and B. Akin, "Spatial Inductance Estimation for Current Loop Auto-Tuning in IPMSM Self-Commissioning," in *IEEE Trans. Ind.*

Electron., vol. 67, no. 5, pp. 3911–3920, May 2020, doi: 10.1109/TIE.2019.2914640.

[11] D. Reigosa, Y. g Kang, M. Martínez, D. Fernández, J. M. Guerrero, and F. Briz, "SPMSMs Sensorless Torque Estimation Using High-Frequency Signal Injection," in *IEEE Trans. Ind. Appl*., vol. 56, no. 3, pp. 2700–2708, May 2020, doi: 10.1109/TIA.2020.2975757.

[12] M. Martinez, D. F. Laborda, D. Reigosa, D. Fernández, J. M. Guerrero, and F. Briz, "SynRM Sensorless Torque Estimation Using High Frequency Signal Injection," in *2019 IEEE 10th International Symposium on Sensorless Control for Electrical Drives (SLED)*, Sep. 2019, pp. 1–5, doi: 10.1109/SLED.2019.8896220.

[13] T. Boileau, N. Leboeuf, B. Nahi*d*-Mobarakeh, and F. Meibody-Tabar, "Online Identification of PMSM Parameters: Parameter Identifiability and Estimator Comparative Study," in *IEEE Trans. Ind. Appl*., vol. 47, no. 4, pp. 1944–1957, Jul. 2011, doi: 10.1109/TIA.2011.2155010.

[14] O. C. Kivanc and S. B. Ozturk, "Sensorless PMSM Drive Based on Stator Feedforward Voltage Estimation Improved With MRAS Multiparameter Estimation," in *IEEE ASME Trans. Mechatron*., vol. 23, no. 3, pp. 1326–1337, Jun. 2018, doi: 10.1109/TMECH.2018.2817246.

[15] Yang Yi, D. M. Vilathgamuwa, and M. A. Rahman, "Implementation of an artificial-neural-network-based real-time adaptive controller for an interior permanent-magnet motor drive," in *IEEE Trans. Ind. Appl*., vol. 39, no. 1, pp. 96–104, Jan. 2003, doi: 10.1109/TIA.2002.807233.

[16] S. J. Underwood and I. Husain, "Online Parameter Estimation and Adaptive Control of Permanent-Magnet Synchronous Machines," in *IEEE Trans. Ind. Electron*., vol. 57, no. 7, pp. 2435–2443, Jul. 2010, doi: 10.1109/TIE.2009.2036029.

[17] J. F. Gieras, Permanent magnet motor technology: design and applications. CRC press, 2009.

[18] F. Briz, M. W. Degner and R. D. Lorenz, "Analysis and design of current regulators using complex vectors," in *IEEE Trans. Ind. Appl*., vol. 36, no. 3, pp. 817-825, May-June 2000, doi: 10.1109/28.845057.

[19] L. Harnefors and H. -P. Nee, "Model-based current control of AC machines using the internal model control method," in *IEEE Trans. Ind. Appl*., vol. 34, no. 1, pp. 133-141, Jan.-Feb. 1998, doi: 10.1109/28.658735.

[20] W. Xu and R. D. Lorenz, "High-Frequency Injection-Based Stator Flux Linkage and Torque Estimation for DB-DTFC Implementation on IPMSMs Considering Cross-Saturation Effects," in *IEEE Trans. Ind. Appl*., vol. 50, no. 6, pp. 3805–3815, Nov. 2014, doi: 10.1109/TIA.2014.2322134.

[21] M. Ganchev, C. Kral, and T. M. Wolbank, "Compensation of Speed Dependence in Sensorless Rotor Temperature Estimation for Permanent-Magnet Synchronous Motor," in *IEEE Trans. Ind. Appl*., vol. 49, no. 6, pp. 2487–2495, Nov. 2013, doi: 10.1109/TIA.2013.2263211.

[22] M. Martinez, D. Reigosa, D. Fernández, J. M. Guerrero and F. Briz, "Enhancement of Permanent-Magnet Synchronous Machines Torque Estimation Using Pulsating High-Frequency Current Injection," in *IEEE Trans. Ind. Appl*, vol. 56, no. 1, pp. 358-366, Jan.-Feb. 2020, doi: 10.1109/TIA.2019.2954297.